



**HAL**  
open science

# A comparison between kinetic theory and particle-in-cell simulations of anomalous electron transport in $E \times B$ plasma discharges

Thomas Charoy, Trevor Lafleur, Antoine Tavant, Pascal Chabert, A. Bourdon

## ► To cite this version:

Thomas Charoy, Trevor Lafleur, Antoine Tavant, Pascal Chabert, A. Bourdon. A comparison between kinetic theory and particle-in-cell simulations of anomalous electron transport in  $E \times B$  plasma discharges. *Physics of Plasmas*, 2020, 10.1063/5.0003978 . hal-02877468

**HAL Id: hal-02877468**

**<https://hal.science/hal-02877468>**

Submitted on 22 Jun 2020

**HAL** is a multi-disciplinary open access archive for the deposit and dissemination of scientific research documents, whether they are published or not. The documents may come from teaching and research institutions in France or abroad, or from public or private research centers.

L'archive ouverte pluridisciplinaire **HAL**, est destinée au dépôt et à la diffusion de documents scientifiques de niveau recherche, publiés ou non, émanant des établissements d'enseignement et de recherche français ou étrangers, des laboratoires publics ou privés.

## A comparison between kinetic theory and particle-in-cell simulations of anomalous electron transport in $\mathbf{E} \times \mathbf{B}$ plasma discharges

T. Charoy,<sup>1, a)</sup> T. Lafleur,<sup>2</sup> A. Tavant,<sup>1, 3</sup> P. Chabert,<sup>1</sup> and A. Bourdon<sup>1</sup>

<sup>1)</sup>*Laboratoire de Physique des Plasmas, CNRS, Ecole polytechnique, Sorbonne Université, 91128 Palaiseau, France*

<sup>2)</sup>*PlasmaPotential-Physics Consulting and Research, Canberra, ACT 2601, Australia*

<sup>3)</sup>*Safran Aircraft Engines, 27208 Vernon, France*

(Dated: 14 May 2020)

Understanding anomalous electron transport in  $\mathbf{E} \times \mathbf{B}$  discharges remains a key challenge in the development of self-consistent models of these systems. It has been shown that short-wavelength, high-frequency, instabilities in the azimuthal  $\mathbf{E} \times \mathbf{B}$  direction may be responsible for increased electron transport due to an enhanced electron-ion friction force. Although a theoretical model based on quasi-linear kinetic theory has previously been proposed to describe this friction force, it has so far only undergone limited validation testing. Here we rigorously assess this theoretical model by comparison with the friction force self-consistently obtained from 2D axial-azimuthal particle-in-cell simulations. The simulation geometry is based on a recently established benchmark configuration for  $\mathbf{E} \times \mathbf{B}$  discharges, and a broad parametric study is performed by varying the magnetic field strength, the discharge current density, and the presence of different neutral collisional processes. Overall the theory is found to be in very good agreement with the simulation results for all cases studied; verifying the underlying physical mechanisms leading to enhanced electron transport. We demonstrate however that the friction force depends sensitively on the shape of the electron velocity distribution function, thus posing significant challenges to fully self-consistent, first principles, modelling of anomalous transport in fluid simulations.

---

<sup>a)</sup>Electronic mail: [thomas.charoy@lpp.polytechnique.fr](mailto:thomas.charoy@lpp.polytechnique.fr)

## I. INTRODUCTION

Cross-field discharges, or  $\mathbf{E} \times \mathbf{B}$  discharges, refer to plasma discharges in which a magnetic field  $\mathbf{B}$  is applied in a direction perpendicular to that of any dominant electric field  $\mathbf{E}$  present in the system. These discharge configurations are used in various applications such as sputtering magnetrons for material processing<sup>1,2</sup>, or Hall-Effect Thrusters (HET) for space propulsion<sup>3,4</sup>. The electric field is often created by imposing an axial potential difference between an anode and a cathode; which is often a source of electrons (either through direct emission as in a hollow cathodes, or due to secondary emission from charged particle bombardment). A radial magnetic field is added to confine these electrons and increase the efficiency of these devices. The cross-field configuration causes the electrons emitted from the cathode to drift with a very high speed (typically around  $10^6$  m.s<sup>-1</sup>) in the azimuthal,  $\mathbf{E} \times \mathbf{B}$ , direction, whereas the heavy ions, which are generally unmagnetised, are simply accelerated axially by the electric field.

Even though  $\mathbf{E} \times \mathbf{B}$  discharges have been extensively studied theoretically<sup>3,5-8</sup>, numerically<sup>9-12</sup> and experimentally<sup>13-16</sup>, some fundamental aspects of their operation are still not well understood. One of the most important issues is related to the electron transport across the magnetic field. Indeed, experiments have shown that this transport is significantly higher than that expected from classical collisional transport processes<sup>17</sup>. Electron-wave scattering from short-wavelength instabilities has been implicated as a possible mechanism leading to this so-called "anomalous" transport<sup>18-20</sup>. However, few experimental diagnostics<sup>21-26</sup> can currently be used to study these predominately azimuthal instabilities, often called Electron Drift Instabilities (EDI). Furthermore, the comparison of theoretical models of the drag force produced by EDIs with fluid simulations using ad-hoc mobilities or collisionalities (derived empirically from experiments) is a challenge, as different parameter scalings can give similar results in fluid codes (i.e. the differences are often within the experimental uncertainty of current diagnostics)<sup>27</sup>. Hence, self-consistent Particle-In-Cell (PIC) simulations appear to be the best tools available to find and test new first principles theoretical models.

Many PIC codes have been developed over the last few years<sup>2,9,11,12</sup> to simulate  $\mathbf{E} \times \mathbf{B}$  discharges, leading to the important need for rigorous validation efforts. A benchmark activity has hence been conducted in which seven independently developed 2D axial-azimuthal PIC codes were successfully compared<sup>28</sup>. For several reasons, this simulation model presents itself as a useful candidate tool to help test and challenge any new theoretical transport models. Firstly,

the simulation domain and operating conditions are clearly specified, and 7 independent research groups have obtained similar results. Secondly, the model is representative of an  $\mathbf{E} \times \mathbf{B}$  discharge, and since an ionization source term is imposed (see Section II), the simulation rapidly reaches a steady state which drastically reduces the computational time. Finally, the influence of specific parameters (such as the magnetic field, the discharge current density or the presence of neutral collisions) on the azimuthal instabilities can easily be tested and understood.

Recently, a model based on aspects of quasi-linear kinetic theory was developed<sup>29</sup> to predict the level of enhanced transport. However, this theory has only been compared with PIC simulations in limited testing at only a single set of operating conditions. In the present paper, we challenge this model more extensively against a broad range of PIC simulation results based on the aforementioned simplified simulation benchmark model. Whereas many different discharge behaviours are obtained with this parametric study, the theoretical model is shown to exhibit good agreement with the PIC results in all cases, which increases the confidence in its validity. Furthermore, by making use of the benchmark simulation configuration for  $\mathbf{E} \times \mathbf{B}$  discharges developed previously<sup>28</sup>, this theoretical model can more easily be tested by other researchers in the community.

The simulations considered here require no additional collisionality parameter and neglect electron-wall collisions. Despite this, they demonstrate "anomalous transport". This paper provides a detailed assessment and comparison with the kinetic theory, and verifies that the anomalous transport produced by EDIs can be well described by it. It also highlights why self-consistently implementing anomalous transport in a fluid model represents a major challenge, as the theory depends sensitively on the details of the electron and ion velocity distribution functions.

The simulation model is described first in Section II, along with the specific parameters that have been varied. Then, the role of the instability-enhanced electron-ion friction force on the axial electron transport is analysed in Section III, by looking at each of the different terms in the azimuthal electron momentum conservation equation. After showing the importance of this friction force and testing previous models for approximating it, the recently developed kinetic model is rederived (adding further simplification steps) explicitly in Section IV and compared with the results of the PIC simulations. Finally, the role of specific ion-neutral collisional processes is analyzed in Section V.

## II. 2D PIC SIMULATIONS

### A. Description of the model

*LPPic*, a 2D-3V Particle-In-Cell Monte Carlo Collision (PIC-MCC) code, is used to simulate the axial ( $x$ ) and azimuthal ( $y$ ) directions of an  $\mathbf{E} \times \mathbf{B}$  discharge with an axial electric field  $\mathbf{E}$  and a radial magnetic field  $\mathbf{B}$ . The simulation model is similar to that described extensively in the 2D axial-azimuthal benchmark of Charoy *et al.*<sup>28</sup> in which the code *LPPic* was verified against 6 other independently developed codes. In what follows, only the main characteristics of the simulation will be given. The reader is referred to Ref. [28] for more extensive details.

As shown in figure 1, a 2D structured Cartesian mesh is used, with an axial length of  $L_x = 2.5$  cm and an azimuthal length of  $L_y = 1.28$  cm. The simulation geometry is similar to a HET, but significantly simplified, with an anode closer (0.75 cm instead of a typical value of 2.5 cm, for example, for the SPT-100 thruster) to the position of maximum radial magnetic field (i.e. the thruster exit plane) and an azimuthal length that accounts for only a small part of the real thruster circumference (1.28 cm instead of around 18 cm), with periodic boundary conditions. A voltage difference is imposed between the anode at a potential of 200 V (and located at  $x = 0$  cm) and the cathode with a potential of 0 V (and located at  $x = 2.4$  cm). Because the radial direction is not considered in 2D axial-azimuthal PIC simulations, there is no way to directly include the hollow cathode. Thus, we only consider the main effect of the hollow cathode by injecting electrons to maintain the discharge current balance; as occurs in a real HET and which has been similarly modelled in previous works<sup>18,31,32</sup>. Hence, electrons are emitted into the domain from the cathode at each time step according to a current equality constraint:  $N_{elec,emitted} = \Delta t \times (I_{a,e} - I_{a,i})$  with  $\Delta t$  the time step,  $I_{a,e}$  and  $I_{a,i}$  respectively the anode electron and ion currents. This cathodic model is known to create a cathode sheath<sup>30</sup>, and hence the electron emission plane has been shifted by 1 mm from the right-hand side domain boundary, and the plasma potential has been rescaled in order to impose a potential of zero at this location, as described in Ref. [28]. The simulation includes electrons, singly charged xenon ions, and for Section V, neutral xenon gas. No artificial scaling factors, such as a reduced ion mass or an increased vacuum permittivity, have been used, so as to correctly preserve all spatial and temporal scales in the plasma.

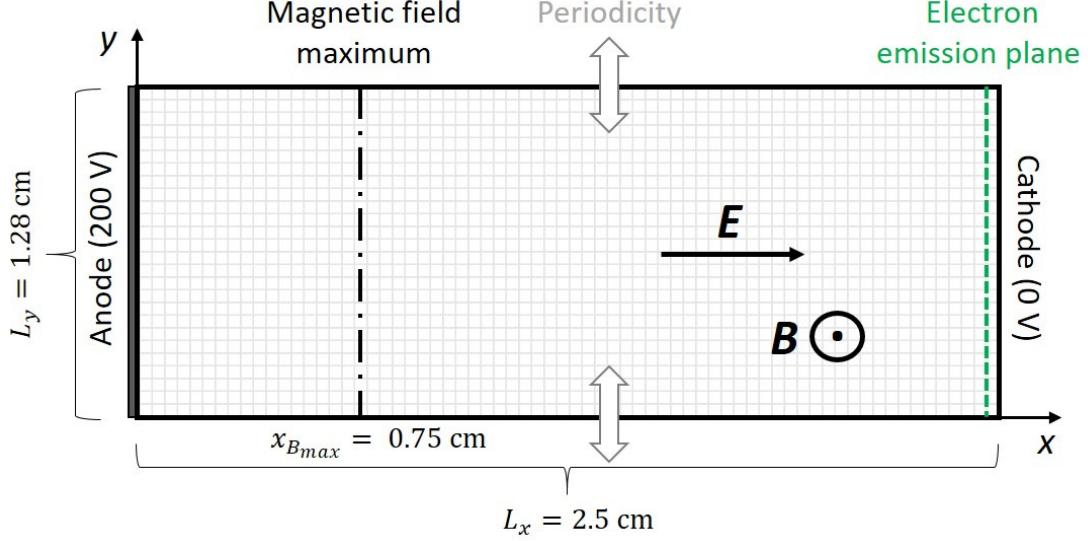


FIG. 1: Simulation domain with  $x$  the axial direction and  $y$  the (periodic) azimuthal direction. Black dotted dashed line ( $x_{B_{max}} = 0.75$  cm): position of the maximum radial magnetic field. Green dashed line ( $x_e = 2.4$  cm): plane from which electrons are emitted uniformly along the azimuthal direction.

The axial profile of the imposed radial magnetic field is shown in figure 2(a), along with the imposed ionization rate profile. In most of the simulations presented here, no neutral collisional processes are taken into account and hence, the discharge needs to be sustained by creating electron-ion pairs according to this cosine-shaped ionization source term. In Section V, the influence of specific ion-neutral collisional processes will be explicitly investigated further. For these tests only, we now include neutral xenon gas (which is treated as a fluid), and use the representative imposed neutral density profile consistent with the ionization source term shown in figure 2(b).

The time step  $\Delta t$  and cell size  $\Delta x$  have been chosen to comply with the PIC stability conditions:  $\Delta t \leq \frac{0.2}{\omega_p}$  and  $\Delta x \leq \lambda_d$  with  $\omega_p = \sqrt{\frac{n_e e^2}{m \epsilon_0}}$  and  $\lambda_d = \sqrt{\frac{\epsilon_0 k_B T_e}{n_e e^2}}$  being respectively the angular plasma frequency and the electron Debye length, with  $n_e$  the electron density,  $e$  the electron charge,  $m$  the electron mass,  $T_e$  the electron temperature,  $k_b$  the Boltzmann constant and  $\epsilon_0$  the vacuum permittivity. The maximum plasma density is  $\approx 5 \times 10^{17} \text{ m}^{-3}$  with an electron temperature of  $\approx 50$  eV, hence a time step  $\Delta t \approx 5 \times 10^{-12}$  s and a grid spacing  $\Delta x \approx 5 \times 10^{-5}$  m are used. The initial number of macroparticles per cell has been set to 75 with an initial uniform plasma density of  $5 \times 10^{16} \text{ m}^{-3}$ , to obtain 250 macroparticles per cell on average at steady state, which gives numerical convergence according to the previous work in Ref. [28].

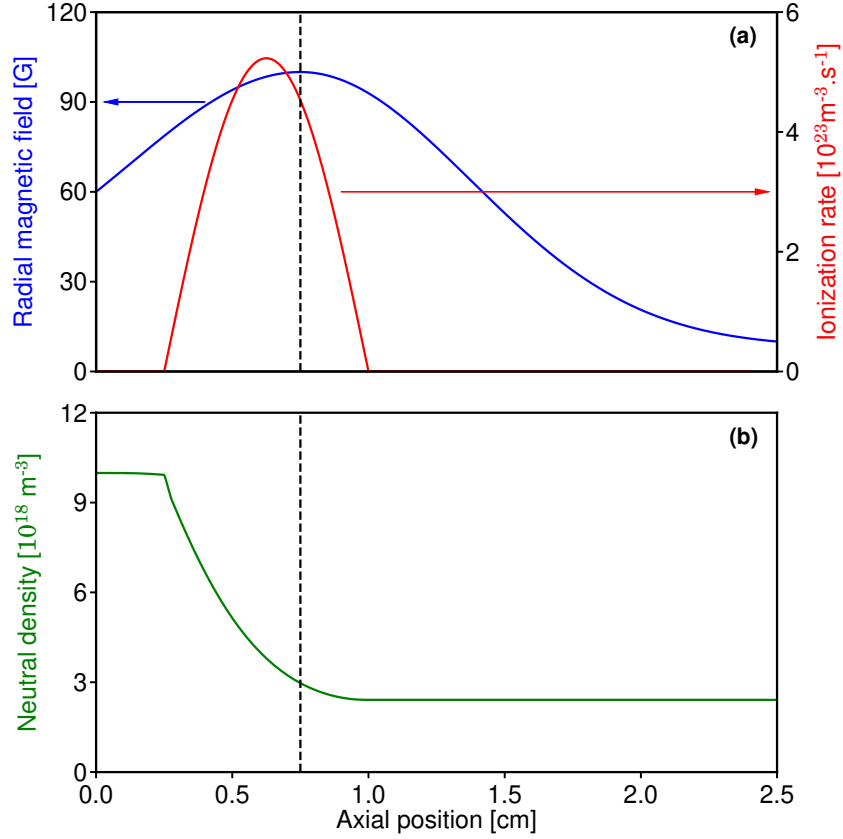


FIG. 2: (a) Axial profiles of the imposed radial magnetic field and ionization rate. (b) Axial profile of the neutral density used for the collisional cases in Section V. The vertical black dashed lines correspond to the position of the maximum magnetic field.

## B. Parametric studies

Several parameters have been varied here. Firstly, the maximum value of the radial magnetic field, which has a nominal value of 100 G, has been changed to 50, 150 and 200 G, while keeping the same axial profile. Then, for the nominal value of 100 G, the current density of  $400 \text{ A} \cdot \text{m}^{-2}$  has been decreased to 200, 100 and  $50 \text{ A} \cdot \text{m}^{-2}$ , which is equivalent to decreasing the plasma density by a corresponding factor. These 7 simulation cases will be used in Sections III and IV. Finally, the effect of ion-neutral collisions (specifically backscattering or isotropic reactions) are studied in Section V. All of the above simulation cases are summarized in Table I.

TABLE I: Simulation cases. Case 0 represents the nominal case.

Case	Magnetic field maximum [G]	Current density [A.m <sup>-2</sup> ]	Collisions
0	100	400	No
1	<b>50</b>	400	No
2	<b>150</b>	400	No
3	<b>200</b>	400	No
4	100	<b>50</b>	No
5	100	<b>100</b>	No
6	100	<b>200</b>	No
7	100	400	<b>Only backscattering</b>
8	100	400	<b>Only isotropic scattering</b>
9	100	400	<b>All collisions</b>

A variation of the radial magnetic field strength is expected to have an influence on the discharge behaviour and more specifically on the azimuthal instabilities observed in the domain. Figure 3 shows contour plots of the azimuthal electric field and ion density at the magnetic field values indicated after the simulations have reached equilibrium (at  $t = 15 \mu\text{s}$ ). As seen, the oscillations exhibit different behaviour depending on the magnetic field strength. The sharp difference between the near-anode region and the plume region (also previously observed for the nominal case ( $B = 100 \text{ G}$ ) in Ref. [28]) is smoothed when the magnetic field is increased: the long-wavelength plume zone seems to extend to the near-anode region. By contrast, when  $B$  is decreased to 50 G, the short-wavelength region seems to extend to the plume.

The sharp change in oscillation wavelength between the near-anode and plume regions is not yet fully understood, particularly since it is only present at low magnetic field strengths. One hypothesis may be that azimuthal waves are predominately excited in the near anode region (where the plasma density maximum occurs), and as these waves propagate downstream, the dominant wavelength changes so that the local dispersion relation is continually satisfied. A similar effect has previously been analysed in the context of collisionless resistive shock waves<sup>33</sup>. Since the plasma density in the downstream region is lowest at the lowest magnetic field, this may explain

why the effect is more prominent at 50 G.

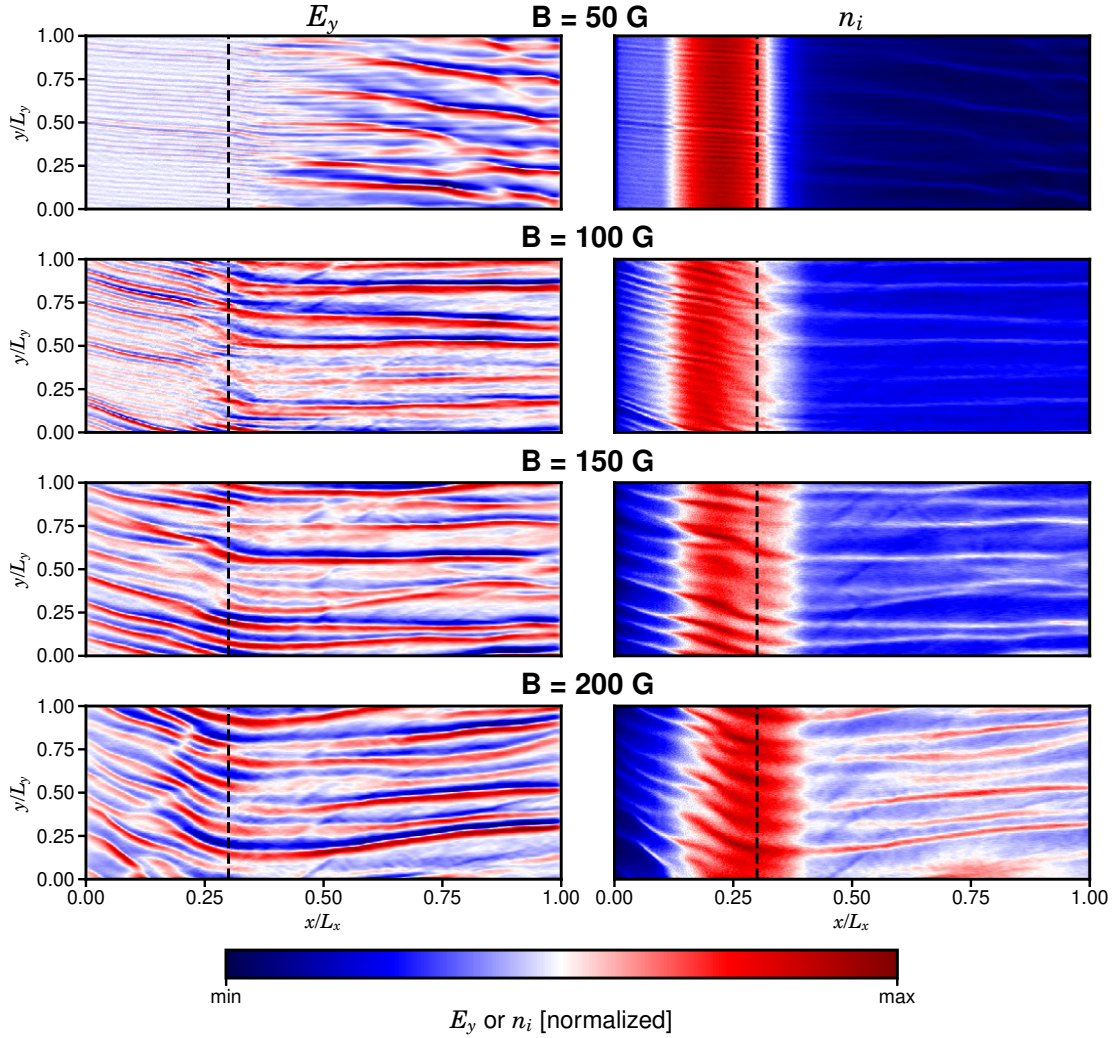


FIG. 3: 2D maps of the azimuthal electric field (left column) and ion density (right column) at  $t = 15 \mu\text{s}$  for different magnetic field strengths. The vertical black dashed lines correspond to the position of the maximum magnetic field.

In figure 4, the results obtained for different current densities are presented. As in the previous work of Boeuf and Garrigues<sup>32</sup>, in which a similar case was simulated, we observe similar behaviour in figure 4: when the current density (and hence the plasma density) is decreased, the wavelength of the azimuthal instabilities increases. This behaviour is expected if the ion-acoustic approximation of the azimuthal instabilities is considered: indeed, for an ion-acoustic instability, the wave number giving the maximum growth rate is<sup>20</sup>:  $k_{max} = (\lambda_d \sqrt{2})^{-1}$ . When the current

density is increased, the plasma density increases, which in turn decreases the Debye length, and hence the instability wavelength decreases.

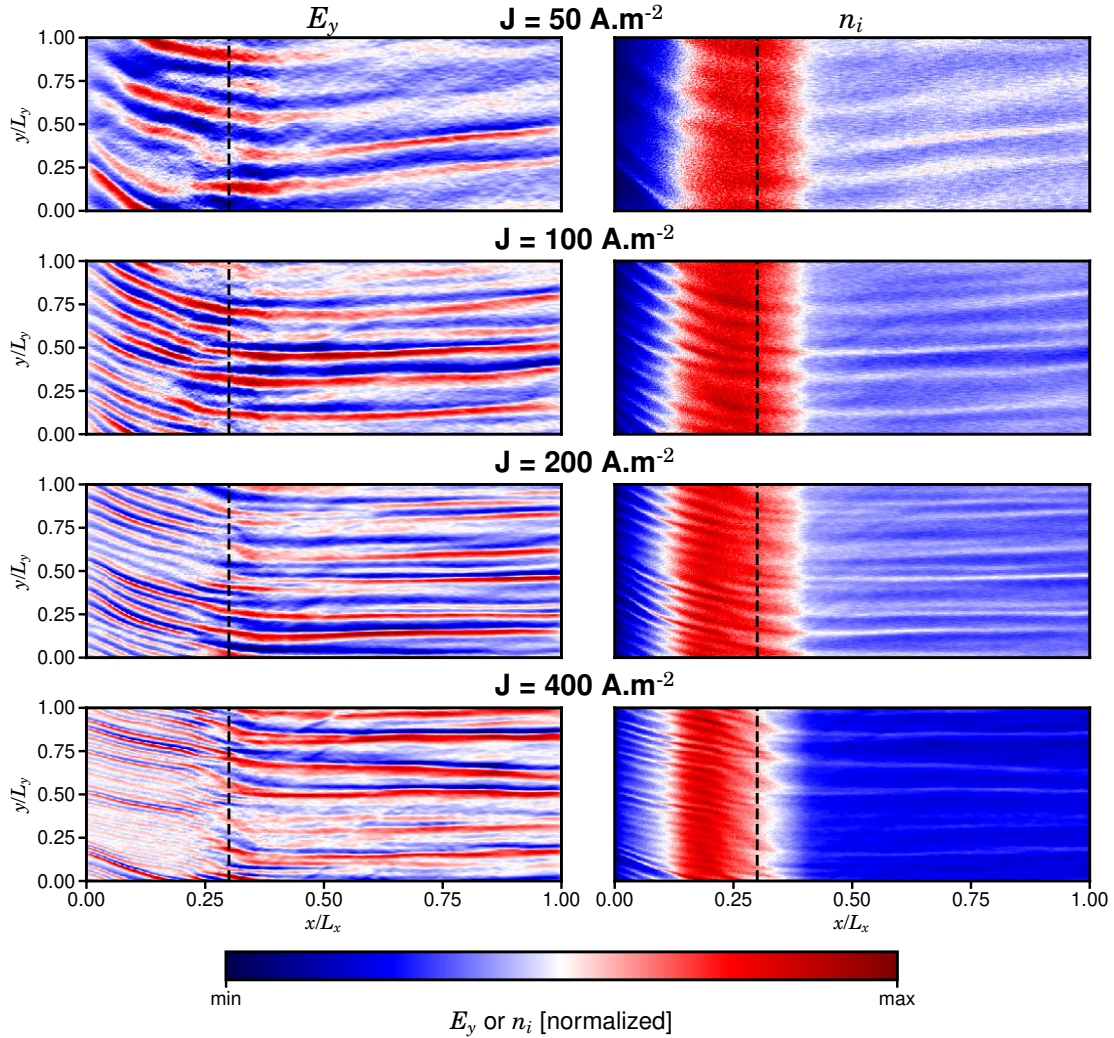


FIG. 4: 2D maps of the azimuthal electric field (left column) and ion density (right column) at  $t = 15 \mu\text{s}$  for different discharge current densities. The vertical black dashed lines correspond to the position of the maximum magnetic field.

For all of the above test cases, the azimuthal instabilities exhibit different characteristics, and hence, they represent a good database to, firstly, compute macroscopic transport terms to better understand the anomalous transport of electrons (as will be discussed in Section III), and secondly, to better challenge first principles theories which seek to quantify the level of cross-field electron transport (as will be discussed in Section IV). It should be noted that in a real HET discharge, the

ionization source term is expected to change when the magnetic field profile or the current density are modified. Hence, it is important to keep in mind the limitation of an imposed ionization source term, which would naturally preclude the existence of certain types of low to mid frequency waves in the discharge, such as the breathing mode, and possibly also any ion transit-time oscillations<sup>34</sup>. Such waves are known to have a large effect on the plasma discharge, which would then affect the growth of any high-frequency azimuthal instabilities. We stress though that the main purpose of the different simulation cases used in this work are focused specifically on a fundamental understanding of the azimuthal waves, and to challenge theoretical models for the resulting anomalous transport over a broad range of discharge behaviours.

### III. ELECTRON-ION FRICTION FORCE

In this section, we focus on the force terms contributing to the electron transport to better understand the cause of the anomalous electron transport in the axial direction.

#### A. Electron-momentum conservation equation

The electron momentum conservation equations can be derived from the electron kinetic equation. As described in detail in Lafleur *et al*<sup>35</sup>, this derivation gives the following equations (averaged over the azimuthal direction, and over short times) in the axial and azimuthal directions, respectively:

$$qn_e v_{e,y} B = \partial_t(mn_e v_{e,x}) + \partial_x(mn_e v_{e,x}^2) + \partial_x(\Pi_{e,xx}) - qn_e E_x - R_{en,x} - R_{ei,x} \quad (1)$$

$$qn_e v_{e,x} B = \partial_t(mn_e v_{e,y}) + \partial_x(mn_e v_{e,x} v_{e,y}) + \partial_x(\Pi_{e,xy}) - qn_e E_y - R_{en,y} - R_{ei,y} \quad (2)$$

with the electron distribution function moments, the electron-neutral collisional momentum loss and the electron-ion friction force respectively defined as:

$$\left\{ \begin{array}{l} n_e = \int_{-\infty}^{\infty} f_e(\mathbf{w}) d^3 w \\ n_e \mathbf{v}_e = \int_{-\infty}^{\infty} \mathbf{w} f_e(\mathbf{w}) d^3 w \\ \Pi_e = m \int_{-\infty}^{\infty} (\mathbf{w} - \mathbf{v}_e)(\mathbf{w} - \mathbf{v}_e) f_e(\mathbf{w}) d^3 w \end{array} \right. \quad (3)$$

$$\mathbf{R}_{en} = -mn_g \int_{-\infty}^{\infty} \sigma_m(w) w \mathbf{w} f_e(\mathbf{w}) d^3 w \quad (4)$$

$$\mathbf{R}_{ei} = q \langle \delta n_e \delta \mathbf{E} \rangle = q \langle [ \langle n_e \rangle_t - n_e(t) ] [ \langle \mathbf{E} \rangle_t - \mathbf{E}(t) ] \rangle_t \quad (5)$$

with  $\sigma_m$  the momentum transfer electron-neutral cross-section and the angled brackets  $\langle \dots \rangle_t$ , a time average.

We can define  $F_{B,x} = qn_e v_{e,y} B$  and  $F_{B,y} = qn_e v_{e,x} B$  respectively as the axial and azimuthal magnetic force terms,  $F_{t,x} = \partial_t(mn_e v_{e,x})$  and  $F_{t,y} = \partial_t(mn_e v_{e,y})$  respectively the axial and azimuthal temporal inertia terms,  $F_{in,x} = \partial_x(mn_e v_{e,x}^2)$  and  $F_{in,y} = \partial_x(mn_e v_{e,x} v_{e,y})$  respectively the axial and azimuthal spatial inertia terms,  $F_{p,x} = \partial_x(\Pi_{e,xx})$  and  $F_{p,y} = \partial_x(\Pi_{e,xy})$  the relevant pressure tensor terms,  $F_{E,x} = -qn_e E_x$  and  $F_{E,y} = -qn_e E_y$  respectively the axial and azimuthal electric force terms,  $F_{en,x} = -R_{en,x}$  and  $F_{en,y} = -R_{en,y}$  respectively the axial and azimuthal electron-neutral momentum collisional drag force terms, and  $F_{ei,x} = -R_{ei,x}$  and  $F_{ei,y} = -R_{ei,y}$  respectively the axial and azimuthal instability-enhanced electron-ion friction force terms. Note that these instability-enhanced force terms are referred to as an "electron-ion friction force", because the force is produced due to the relative drift between electron and ion species, and acts to decrease the electron drift speed, while increasing the ion drift speed. This is completely analogous to the drag force experienced by two gases drifting through each other. An important implication of the word "friction", is that the electron-ion force term should be equal and opposite to the ion-electron force term. This is explicitly demonstrated in Section [IV D](#) below. A similar analysis relating wave properties to an effective drag force density term in the fluid conservation equations has also been performed by Davidson and Krall<sup>36</sup> in the context of ion acoustic waves in high-temperature discharges with cross-field currents.

Axial profiles of the different terms in equations [1](#) and [2](#) are shown in figure [5](#) for the nominal case. In the axial direction (figure [5\(b\)](#)), we retrieve the behaviour observed in Ref. [[32](#)]: only the pressure gradient term (diamagnetic term)  $F_{p,x}$  and the axial electric field term  $F_{E,x}$  contribute to the electron drift, the former being dominant near the anode while the latter being dominant near the exit plane. As expected, the amplitude of the force terms is orders of magnitude higher than in the azimuthal direction: electrons have an axial velocity that is negligible compared to the azimuthal drift velocity. The above results are also in agreement with those obtained in Ref. [[35](#)]

While the PIC simulations correctly resolve long-range electron-ion collisional effects with a

wavelength of the order of the Debye length or greater, short-range Coulomb collisions are not explicitly modelled. It is nonetheless interesting to evaluate the expected friction force density from such Coulomb collisions, and compare it with the instability-enhanced friction force density obtained in the simulations. As discussed in further detail in Ref. [37], the classical electron-ion friction force in a stable plasma can be found from the momentum moment of the Lenard-Balescu equation<sup>38,39</sup>, which for singly charged ions and a quasi-neutral plasma yields

$$F_{ei}^{LB} \approx \frac{2.7n_e^2|q|^3 \ln\Lambda}{(4\pi\epsilon_0)^2 T_e} \quad (6)$$

where  $\ln\Lambda$  is the Coulomb logarithm. This force density is shown in figure 5(a), and as expected, is found to be negligible compared to the instability-enhanced friction force. It is interesting to note that the difference in magnitude (of the order of a factor of 500) is similar to that estimated theoretically in previous work<sup>37</sup>.

The azimuthal direction, shown in figure 5(a), is of more interest as the left-hand side of equation 2 corresponds to the electron axial velocity and hence the right-hand side displays all of the terms that contribute to the axial transport. We observe that the instability-enhanced friction force  $F_{ei,y}$  is the main contributor to the axial electron transport, and that this leads to cross-field electron transport even in the absence of electron-wall or electron-neutral collisions. In previous work<sup>35</sup> which used a self-consistent PIC simulation, the terms of the electron momentum balance equation were similarly evaluated, and the spatial inertia  $F_{in,y}$  and pressure  $F_{p,y}$  terms in the azimuthal direction were found to be very small. Observation of figure 5 shows that these terms become relatively large at the location where the imposed ionization profile first starts (when moving towards the anode region). Since electrons are continually, and artificially, added into the simulation in the ionization region, and since in general these electrons have a different temperature and velocity distribution function compared to the other self-consistently evolved simulation electrons, the azimuthal inertia and pressure terms (which are off-diagonal tensor terms), may undergo a sudden change. Such a change may not be otherwise observed if all electrons and collisional processes were evolved smoothly and self-consistently.

## B. PIC results for different operating conditions

The azimuthal electron momentum force terms for simulation cases with different magnetic field strengths and current densities are shown in figure 6 (the force terms  $F_{t,y}$ ,  $F_{E,y}$  and  $F_{en,y}$  are

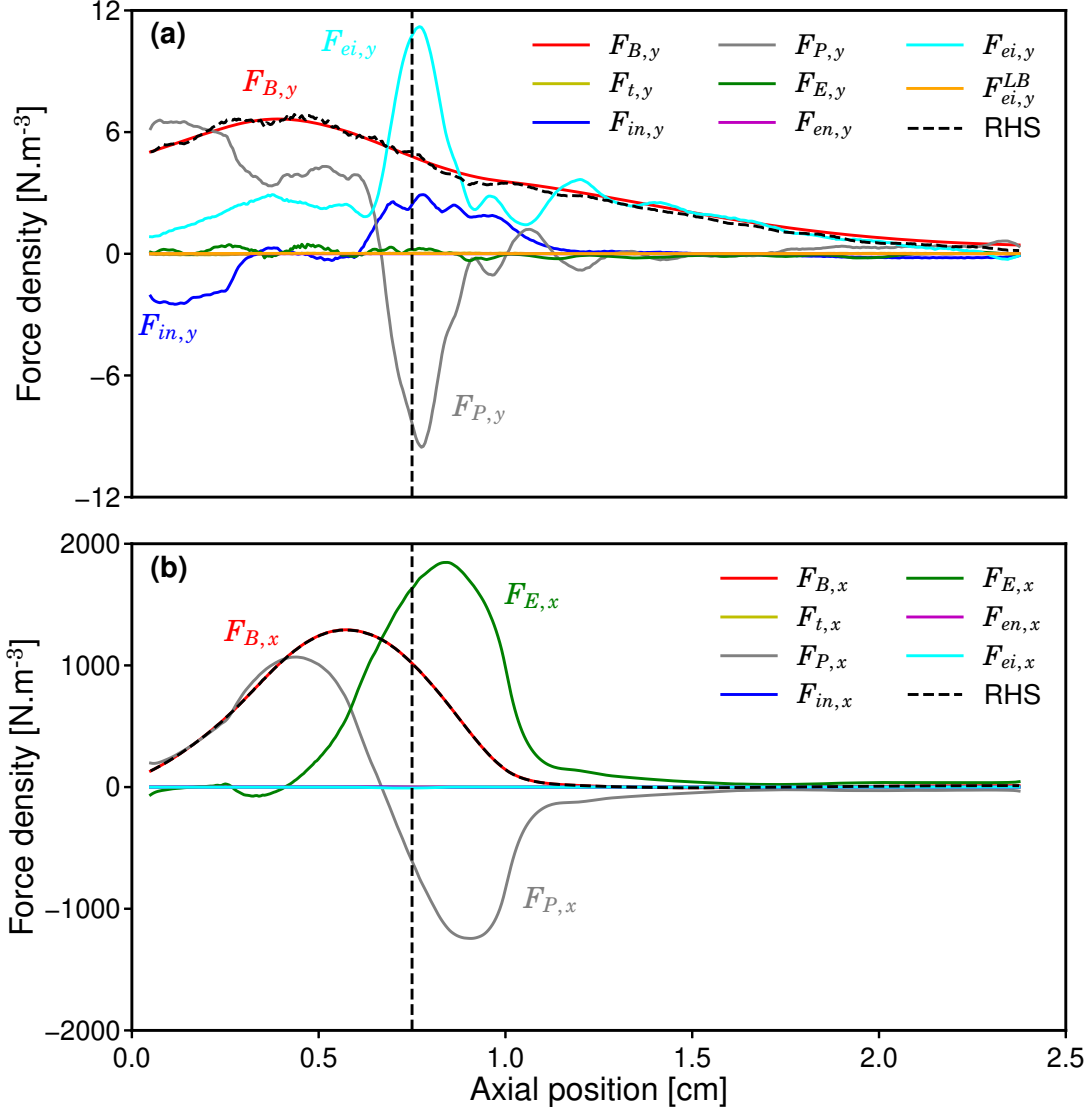


FIG. 5: Electron momentum force density terms for the nominal case ( $B = 100$  G and  $J = 400$  A.m<sup>-2</sup>) in the azimuthal direction (a) and the axial direction (b). The curves labelled "RHS" represent the sum of all of the individual terms on the right-hand side of equations 1 and 2. The vertical black dashed lines correspond to the position of the maximum magnetic field.

negligible and hence, they are not displayed for the sake of clarity). One can note that the force terms exhibit a broad range of magnitudes, and for all configurations, the electron-ion friction force is the main contributor to the axial electron transport. The dependence on the current density observed in Section II B is retrieved here: when the current density (and hence the plasma density) is decreased, the electron-ion friction force decreases, together with the overall axial electron transport. This is expected because the oscillation amplitude of the azimuthal instabilities is also

decreased when the current density decreases, and the friction force is proportional to this amplitude (as seen in the next section with equation 24). One can see that there is a direct correlation for this decrease: when the current density is divided by 2, the electron-ion friction force is also divided by 2. The trend for the magnetic field variations is less clear. It seems that the electron-ion friction force increases when the magnetic field increases, with a distinct peak occurring in the plume when  $B = 50$  G.

For different configurations, the instability-enhanced electron-ion friction force has been observed to be the main cause of the axial electron transport. Hence, it highlights the importance of finding an approximate model for this force term that can be added to fluid codes to more self-consistently model anomalous electron transport.

## IV. THEORETICAL MODELS FOR ENHANCED ELECTRON TRANSPORT

### A. Theoretical models

The prediction of the anomalous collision frequency (and hence, of the force term leading to enhanced transport) is crucial for fluid and hybrid models. In the previous decade, many attempts have been made to find an accurate and flexible model<sup>20,40–42</sup>. Four models have been selected here to be compared with the PIC results for the nominal simulation case. The kinetic theory model developed in Ref. [29] is further detailed and tested more extensively with the different simulation cases described in Section II B.

#### *Empirical model*

One of the first models that was developed is based on Bohm diffusion, which gives the formula<sup>43</sup>:

$$v_{bohm} = \frac{K}{16} \omega_{ce} \quad (7)$$

with  $\omega_{ce} = \frac{qB}{m}$  the electron cyclotron frequency and  $K$  an empirical parameter. Hagelaar *et al.*<sup>40</sup> have used this Bohm approximation in the plume region of a two-dimensional hybrid model and managed to qualitatively reproduce the experimental ionization oscillations and their parameter scalings, along with a good estimation of the thrust<sup>44</sup>. In the thruster chamber, they considered the

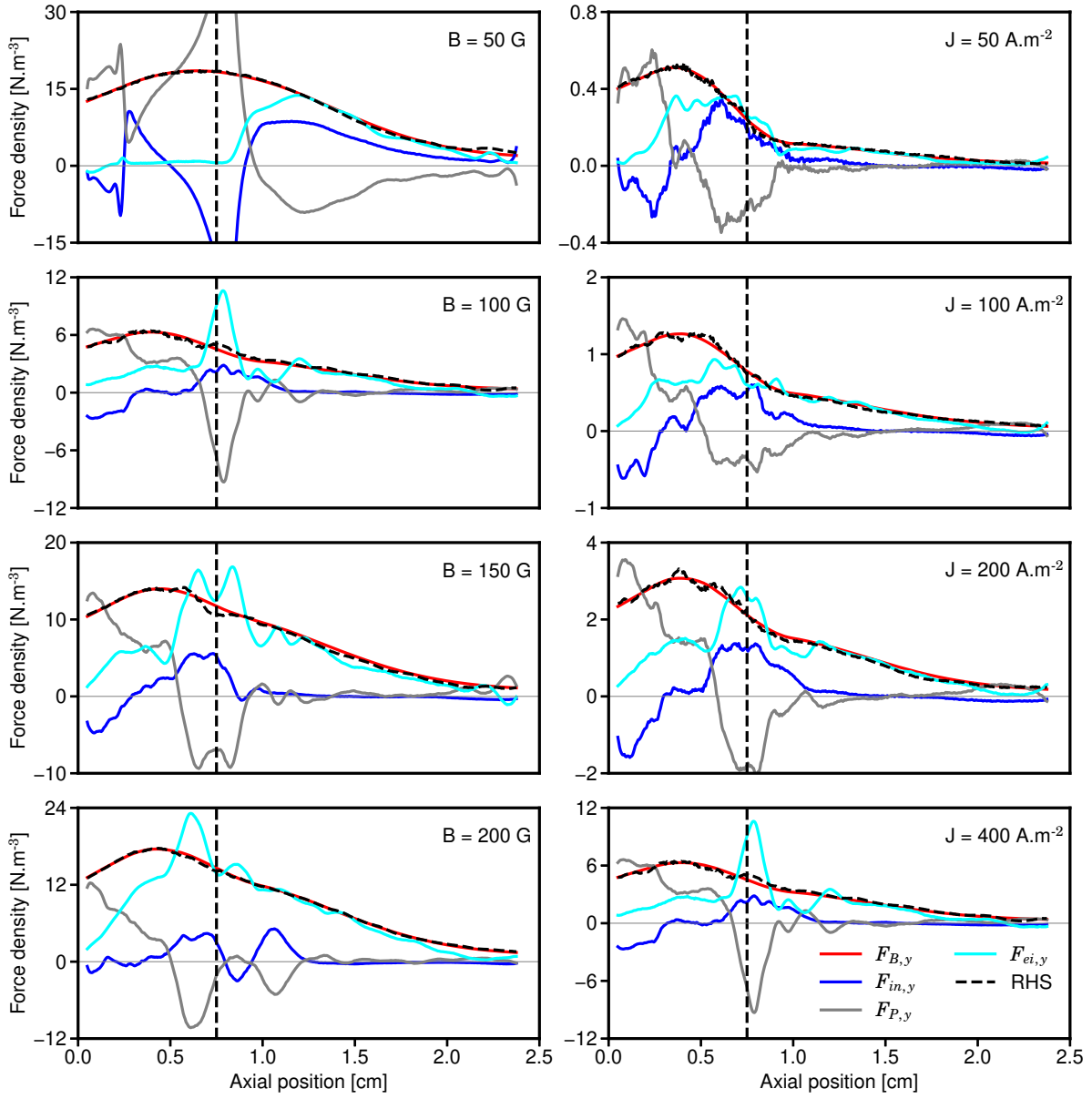


FIG. 6: Azimuthal electron momentum terms for different magnetic fields with  $J = 400 \text{ A.m}^{-2}$  (left column) and current densities with  $B = 100 \text{ G}$  (right column). The nominal case, shown in figure 5(a), corresponds to  $B = 100 \text{ G}$  and  $J = 400 \text{ A.m}^{-2}$ . The vertical black dashed lines correspond to the position of the maximum magnetic field. The force terms  $F_{t,y}$ ,  $F_{E,y}$  and  $F_{en,y}$  are not shown for the sake of clarity but are still included in the curve labelled "RHS" that represent the sum of all of the individual terms on the right-hand side of equations 2.

effect of the walls by using a different empirical formula:

$$v_{wall} = \alpha v_{ref} \quad (8)$$

with  $v_{ref} = 10^7 \text{ s}^{-1}$  a reference frequency for wall collisions and  $\alpha$  an additional empirical parameter. One can notice that empirical models are usually formulated in terms of collision frequencies. Hence, the corresponding anomalous force term is:

$$\begin{cases} R_{an,empirical} = -mn_e v_{e,y} \alpha v_{ref} & (\text{inside}) \\ R_{an,empirical} = -n_e v_{e,y} \frac{K}{16} qB & (\text{outside}) \end{cases} \quad (9)$$

Other empirical models can be found in the literature, such as those based on machine-learning developed by Jorns<sup>42</sup>, but we have selected only a single representative model here for clarity.

### ***Quasi-linear kinetic theory with ion-trapping saturation***

In Lafleur *et al.*<sup>20</sup>, a kinetic theory was developed which explained the anomalous transport in terms of an instability-enhanced friction force, with the azimuthal instabilities saturating due to ion-wave trapping. Taking into account a more accurate ion-trapping magnitude which comes from Ref. [35], the force can be written as:

$$R_{ei,saturated} = \frac{q}{16\sqrt{6}c_s} |\nabla(v_{i,x} n_e T_e)| \quad (10)$$

where  $c_s$  is the ion sound speed,  $v_{i,x}$  the axial ion drift velocity and  $T_e$  the electron temperature expressed in eV. This formula was shown to match the empirical electron mobility profile needed in fluid simulations to get agreement with experiments<sup>15,20</sup>, and was further used by Croes *et al.*<sup>45</sup> in which good agreement was found for 2D radial-azimuthal PIC simulations (in which the observed instabilities saturated at a similar level to that predicted by ion-wave trapping).

### ***Quasi-linear kinetic theory***

In Ref. [29] a quasi-linear kinetic model for the instability-enhanced force was derived. A similar approach has been used by Davidson and Krall<sup>36</sup> in the context of ion acoustic waves in discharges with cross-field currents. This derivation is given here in more detail, and extended by further simplification steps allowing a more transparent and compact formula. Considering the

equations of quasi-linear kinetic theory, the anomalous friction force density,  $\mathbf{R}_{ei}$ , can be written as<sup>20,29</sup>

$$\mathbf{R}_{ei} = q \langle \delta n_e \delta \mathbf{E} \rangle \quad (11)$$

where  $\delta n_e$  is the perturbed electron density, and  $\delta \mathbf{E}$  is the perturbed electric field. By taking the Fourier transform of the perturbed Vlasov equation, and considering only a single dominant wave mode, Eq. 11 can be written as<sup>29</sup>

$$\mathbf{R}_{ei} = -\frac{e^2 \mathbf{k} |\delta \mathbf{E}|^2}{2mk^2} \text{Im} \left\{ \int_{-\infty}^{\infty} d^3 v \frac{\mathbf{k} \cdot \nabla_v f_{e0}}{\omega - \mathbf{k} \cdot \mathbf{v}} \right\} \quad (12)$$

Here  $\mathbf{k}$  and  $\omega$  are the instability wavevector and complex frequency,  $\mathbf{v}$  is the electron velocity phase space coordinate,  $f_{e0}$  is the equilibrium (i.e. time-averaged over the short time scales of the instability) Electron Velocity Distribution Function (EVDF), and  $\nabla_v$  is the gradient operator with respect to the velocity.

Equation 11 has been derived using a number of important assumptions that are worth highlighting further. Firstly, since the PIC simulations are electrostatic, only electrostatic instabilities have been considered in the theory so as to allow a more relevant comparison. This does not however necessarily mean that electromagnetic modes are not important; only that we are not yet able to test or investigate this further. Some experimental measurements<sup>46</sup> have observed magnetic field fluctuations in HETs, suggesting that electromagnetic modes may be present. Secondly, we have made use of a linear dielectric response function for the plasma which considers unmagnetized electrons. Rigorous justification for the validity of quasi-linear theory can often be challenging to establish, but a typical approximate criterion is that the level of potential energy fluctuations be much less than the thermal energy of the plasma, i.e.  $\frac{\delta \phi}{T_e} \ll 1$ . From Section IV B, this criterion is well satisfied everywhere in the plasma. However, since the instabilities appear to saturate, and ion wave trapping is observed, nonlinear effects may well be important in some regions of the discharge. In this case, the use of a linear dielectric response function would seem unjustified, and since a reasonably strong magnetic field is present, so would the assumption of unmagnetised electrons. Lampe et al.<sup>47</sup> have analysed the nonlinear evolution of beam-cyclotron instabilities (similar to the electron cyclotron drift instability considered here), and by considering magne-

tised electrons and an approximate nonlinear plasma dielectric response function, showed that a transition to an unmagnetised, linear ion acoustic instability occurs. The large amplitude, largely coherent nonlinear wave acts to “smear” out the electron cyclotron resonances, and the plasma is left with its ion acoustic character. This fortuitous result allows us to consider the electrons as unmagnetised, and to use the much simpler linear plasma dielectric response function, from which we obtain equation 11. In this case, the only role of the magnetic field is in providing the large azimuthal electron drift velocity which drives the instability.

If we consider now an instability that is predominately in the azimuthal ( $y$ ) direction, the friction force in the azimuthal direction (that will be noted  $R_{ei}$  in the following for the sake of clarity) can then be simplified to give

$$R_{ei} = \frac{e^2 n_e |\delta \mathbf{E}|^2}{2mk_y} \text{Im} \left\{ \int_{-\infty}^{\infty} dv_y \frac{\frac{dF_{e0}}{dv_y}}{v_y - \zeta} \right\} \quad (13)$$

where  $\zeta = \frac{\omega}{k_y}$  is the instability phase velocity, and where

$$F_{e0}(v_y) = \frac{1}{n_e} \int_{-\infty}^{\infty} dv_x dv_z f_{e0}(\mathbf{v}) \quad (14)$$

with  $n_e$  the time-averaged electron density. Thus  $\int_{-\infty}^{\infty} dv_y F_{e0}(v_y) = 1$ . We can define the energy density of the wave electric field,  $\epsilon_{wave}$ , as

$$\epsilon_{wave} = \frac{1}{2} \epsilon_0 \langle |\delta \mathbf{E}| \rangle_{rms}^2 = \frac{1}{4} \epsilon_0 |\delta \mathbf{E}|^2 \quad (15)$$

where the subscript refers to the Root Mean Square (RMS) value, defined as:

$$\langle \delta \mathbf{E} \rangle_{rms} = \sqrt{\frac{1}{L_y} \int_0^{L_y} (\delta E_x^2 + \delta E_y^2) dy} \quad (16)$$

Using Eq. 15 in Eq. 13, and simplifying, we obtain

$$R_{ei} = \frac{2\omega_{pe}^2 \epsilon_{wave}}{k_y} \text{Im} \left\{ \int_{-\infty}^{\infty} dv_y \frac{\frac{dF_{e0}}{dv_y}}{v_y - \zeta} \right\} \quad (17)$$

The simplified ion-acoustic dispersion relation can be expressed as<sup>20,37</sup>:

$$\omega_R \approx \mathbf{k} \cdot \mathbf{v}_{di} \pm \frac{kc_s}{\sqrt{1 + k^2 \lambda_{De}^2}} \quad (18)$$

$$\gamma \approx \pm \sqrt{\frac{\pi m}{8M}} \frac{\mathbf{k} \cdot \mathbf{v}_{de}}{(1 + k^2 \lambda_{De}^2)^{3/2}} \quad (19)$$

with  $\mathbf{v}_{de}$  and  $\mathbf{v}_{di}$  the azimuthal electron and ion drift velocities respectively and  $M$  the ion mass.

From these relations, the maximum growth rate occurs for  $k_y \lambda_{De} = \frac{1}{\sqrt{2}}$ . Thus Eq. 17 becomes

$$R_{ei} = 2\sqrt{2}\omega_{pe}^2 \lambda_{De} \epsilon_{wave} \text{Im} \left\{ \int_{-\infty}^{\infty} dv_y \frac{\frac{dF_{e0}}{dv_y}}{v_y - \zeta} \right\} \quad (20)$$

If we focus now on the integral term, the Plemelj relation gives

$$\int dx \frac{g(x)}{x - \zeta} = \text{P} \int dx \frac{g(x)}{x - \zeta} + i\pi g(\zeta) \quad (21)$$

with  $\text{P}$  denoting the Cauchy principal value. Thus, we can write the integral term in Eq. 20 as

$$\int_{-\infty}^{\infty} dv_y \frac{\frac{dF_{e0}}{dv_y}}{v_y - \zeta} = \text{P} \int_{-\infty}^{\infty} dv_y \frac{\frac{dF_{e0}}{dv_y}}{v_y - \zeta} + i\pi \left. \frac{dF_{e0}}{dv_y} \right|_{v_y=\zeta} \quad (22)$$

Thus Eq. 20 simplifies to

$$R_{ei} = 2\sqrt{2}\pi\omega_{pe}^2 \lambda_{De} \epsilon_{wave} \left. \frac{dF_{e0}}{dv_y} \right|_{v_y=\zeta} \quad (23)$$

Therefore, if the normalised time-averaged electron distribution function is known, the derivative at the instability phase velocity can be used to determine the anomalous friction force. We can go slightly further by noting that the instability phase velocity is typically of the order of the ion sound speed,  $\zeta \sim c_s = \sqrt{\frac{eT_e}{M}}$ . Since the ion sound speed is much smaller than the electron thermal velocity, Eq. 23 simplifies to

$$R_{ei,quasi-linear} = 2\sqrt{2}\pi\omega_{pe}^2 \lambda_{De} \epsilon_{wave} \left. \frac{dF_{e0}}{dv_y} \right|_{v_y=0} \quad (24)$$

This dependence of particle transport on the derivative of the velocity distribution function is a common feature of quasi-linear theory, which shows the presence of velocity space diffusion<sup>48–50</sup>, and has been applied, for example, to streaming instabilities in both high-temperature and low-temperature plasmas<sup>36,51–53</sup>.

### *Quasi-linear kinetic theory with a Maxwellian Electron Velocity Distribution Function*

If the EVDF is a Maxwellian, we have that

$$F_{e0} = \frac{1}{\sqrt{\pi}v_{Te}} \exp \left[ -\frac{(v - v_{de})^2}{v_{Te}^2} \right] \quad (25)$$

where  $v_{Te} = \sqrt{\frac{2eT_e}{m}}$  is the electron thermal velocity. Thus for a Maxwellian, the anomalous friction force from Eq. 23 becomes

$$R_{ei,maxwellian} = -4\sqrt{2\pi}\omega_{pe}^2\lambda_{De}\epsilon_{wave} \frac{(\zeta - v_{de})}{v_{Te}^3} \exp \left[ -\frac{(\zeta - v_{de})^2}{v_{Te}^2} \right] \quad (26)$$

Since  $\zeta \sim c_s \ll v_{de}$ , Eq. 26 simplifies to give

$$R_{ei,maxwellian} = 4\sqrt{2\pi}\omega_{pe}^2\lambda_{De}\epsilon_{wave} \frac{v_{de}}{v_{Te}^3} e^{-v_{de}^2/v_{Te}^2} \quad (27)$$

### **B. Comparison with the nominal simulation case**

In figure 7, the axial profile of the measured electron-ion friction force for the nominal case is displayed, along with the models described above: the empirical model  $R_{ei,empirical}$  (Eq. 9), the ion-trapping saturation model  $R_{ei,saturated}$  (Eq. 10) and the Maxwellian approximation  $R_{ei,maxwellian}$  (Eq. 27). The more general non-Maxwellian model,  $R_{ei,quasi-linear}$  (Eq. 24), will be discussed in more detail later. The values of the two empirical parameters  $\alpha$  and  $K$  for  $R_{ei,empirical}$  have been set to 0.4 and 0.17 respectively, in order to obtain the best fit. While  $R_{ei,saturated}$  behaves quite differently than the PIC results near the thruster exit,  $R_{ei,maxwellian}$  exhibits a similar shape but overestimates the force density by a factor of about 3.  $R_{ei,maxwellian}$  also changes direction between

about  $x = 1.25$  cm and  $x = 1.75$  cm. The empirical formula seems to match quite well for  $x < 1$  cm, but the coefficients  $\alpha$  and  $K$  have been adjusted here to best-fit the PIC data, and hence this model is not predictive. Furthermore, this model assumes that the anomalous transport inside the thruster is largely due to electron-wall collisions, which are completely absent in the PIC simulation. One can also notice that  $R_{ei,empirical}$  quickly goes to zero in the plume, whereas the PIC values still remain significant. Overall, none of these three formulae accurately matches the measured friction force throughout the simulation domain. Although we only show the comparison in figure 7 for the nominal simulation case, similar results are obtained for the other simulation cases.

The discrepancies observed in figure 7 are expected to occur because of either simplifying assumptions used, or because of the incomplete or ad hoc nature of the models themselves. To gain further insight into why these models do not fit well with the simulation results, we focus now on checking some of the main assumptions used. For example,  $R_{ei,maxwellian}$  assumes that the electron distribution is described by a drifting Maxwellian, while  $R_{ei,saturated}$  assumes that the EDI saturates everywhere in the discharge due to ion-wave trapping.

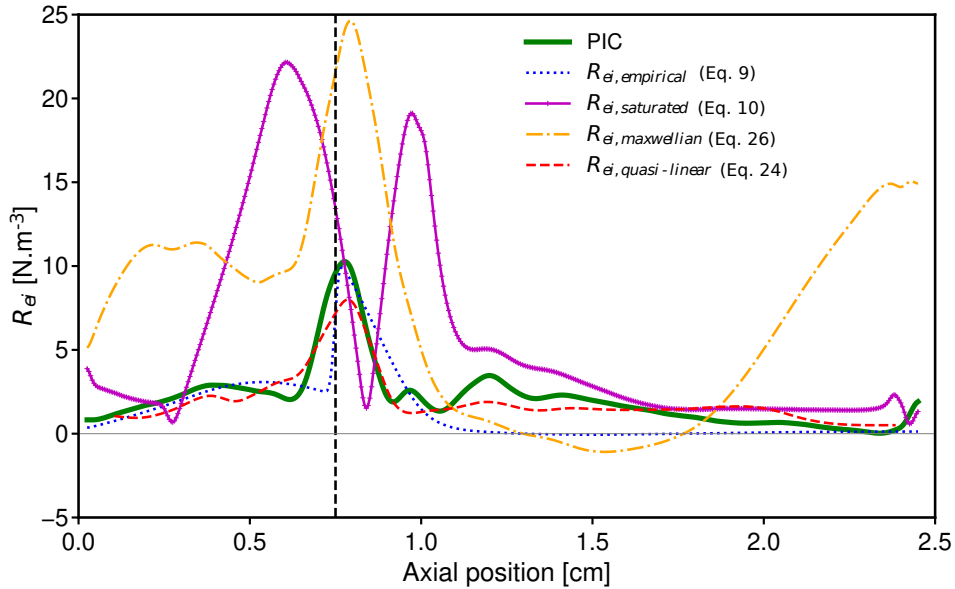


FIG. 7: Comparison of the anomalous force approximations with the PIC simulation results for the nominal case. The vertical black dashed line corresponds to the position of the maximum magnetic field.

EVDFs obtained directly from the PIC simulations for the nominal case are shown in figure 8. Similarly to the other variables used in this work, these distribution functions have been averaged

azimuthally, and in time over 5000 time steps, which significantly reduces any statistical noise. We can see that in the axial and azimuthal directions, the distributions are strongly non-Maxwellian, especially in the near-anode region. Since the friction force depends on the exact details of the electron distribution function<sup>35</sup>, this explains why equation 27 is not a good approximation.

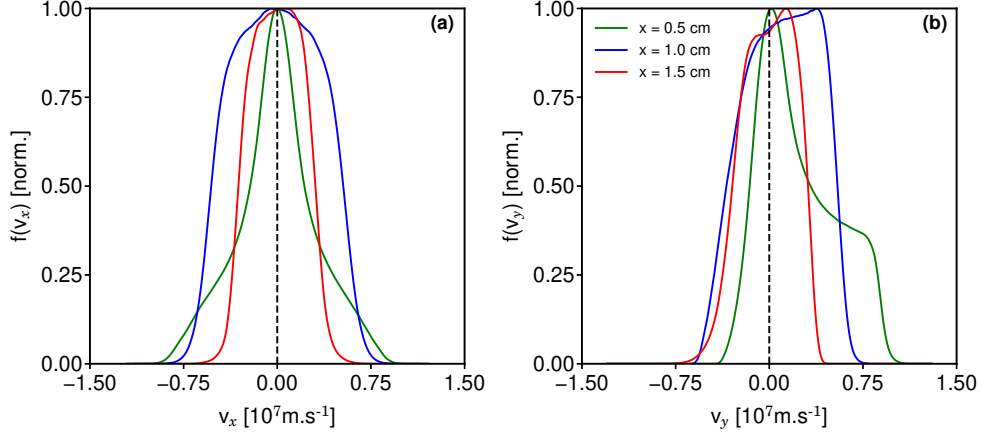


FIG. 8: Electron Velocity Distribution Functions in the axial (a) and azimuthal (b) directions for the nominal simulation case at different axial positions. The vertical black dashed line splits the negative and positive velocities.

Along with the energy density of the wave electric field  $\epsilon_{wave}$  defined in Eq. 15, we can define the electron thermal energy density  $\epsilon_{th}$  as:

$$\epsilon_{th} = \frac{3}{2} n_e T_e \quad (28)$$

For an instability that saturates due to ion-wave trapping, the rms electric field amplitude is<sup>35</sup>:  $\langle |\delta \mathbf{E}| \rangle_{rms} = \frac{T_e}{12 \lambda_d}$ . This gives an upper limit to the wave energy density ratio:

$$\frac{\epsilon_{wave}}{\epsilon_{th}} = \frac{1}{432} \quad (29)$$

The axial profiles of wave energy density ratio, along with the above ion-wave trapping saturation limit, are shown in figure 9 for different magnetic field strengths and discharge current densities. Except for the case with  $B = 50$  G, the wave energy density ratio is below the saturation limit, which is reached near the cathode when the current density is sufficiently high ( $400 \text{ A.m}^{-2}$ ). These results agree with that obtained previously<sup>35</sup>, and explain why equation 10 overestimates the friction force.

While the wave energy seems to increase with higher current density in the plume, the trend is reversed inside the thruster. Although large amplitude azimuthal instabilities have been observed in a number of other PIC simulations<sup>45,54–56</sup>, the fluctuation levels of these instabilities,  $\frac{\langle \delta n_e \rangle}{n_e}$ , are in the range of 15-20%, which is in apparent poor agreement with those measured experimentally downstream of HETs<sup>24</sup> where values of about 1% are found. In comparison to these previous PIC simulations (which do not include the axial thruster direction, and hence do not correctly account for wave convection), other 2D PIC axial-azimuthal PIC simulations<sup>35</sup>, as well as the present simulations, observe a fluctuation level that varies spatially in the discharge. Within the thruster itself, the fluctuation level is about 10%, but this decreases to only a few percent just downstream of the thruster exit, which is very close to previous experimental measurements<sup>24</sup> made in this region. Further downstream of the exit, the fluctuation level again rises, reaching maximum values of the order of 10%. Thus, the fluctuation level shows a strong spatial dependence, and any comparison with experiment needs to account for this. More recent experimental measurements using an improved setup<sup>57</sup>, have observed values as high as 8.7% in a smaller thruster.

We can consider now the more general non-Maxwellian force model,  $R_{ei,quasi-linear}$ . Although equation 24 allows the friction force to be calculated for a non-Maxwellian distribution, the model is incomplete because there is no easy self-consistent way in which to actually determine this distribution function (and similarly for the wave energy density). Nonetheless, the basic physics of this model can be tested by using the local EVDFs and wave energy densities obtained directly from the PIC simulations.  $R_{ei,quasi-linear}$  is shown in figure 7 and we retrieve very well the behaviour of the measured friction force for the nominal simulation case, in both the near-anode region, and the plume.

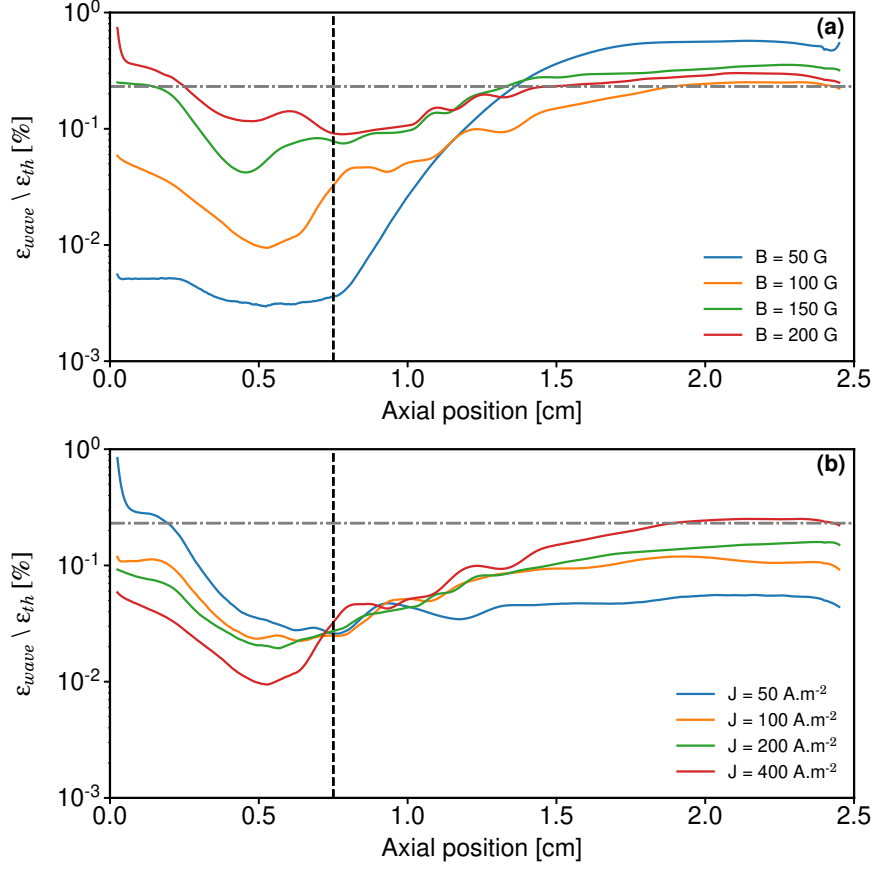


FIG. 9: Ratio of the time-averaged wave energy density to the electron thermal energy density as a function of axial position for different magnetic fields strengths with  $J = 400 \text{ A.m}^{-2}$  (a), and discharge current densities with  $B = 100 \text{ G}$  (b). The horizontal grey dot-dashed line corresponds to the ion-wave trapping saturation limit. The vertical black dashed lines correspond to the position of the maximum magnetic field.

**C. Comparison with parametric PIC results of the friction force derivation accounting for non-Maxwellian electrons**

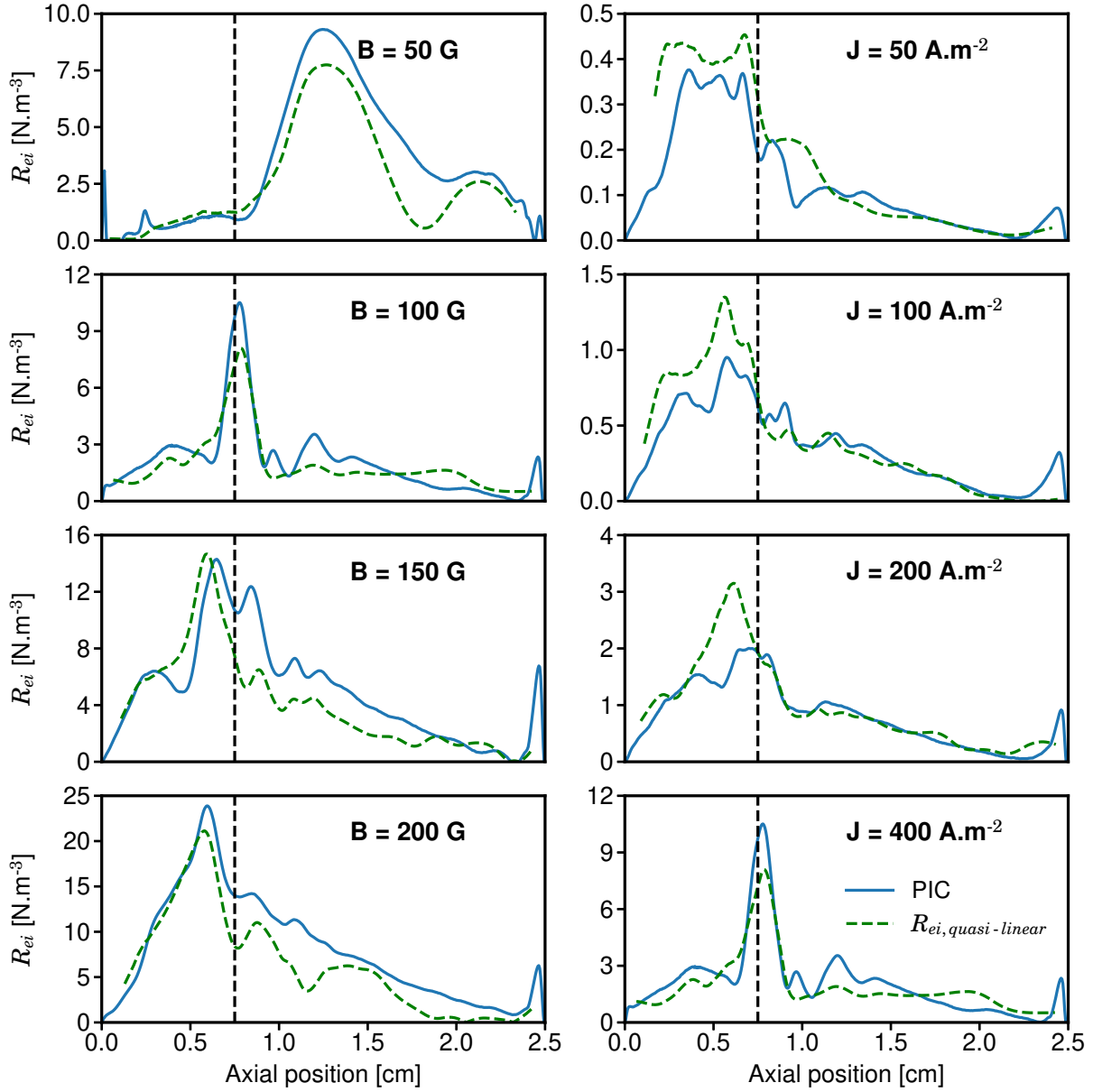


FIG. 10: Friction force as a function of axial position for different magnetic field strengths (left column) and discharge current densities (right column). The blue thick line corresponds to the PIC results, while the green dashed line corresponds to the Non-Maxwellian approximation. The vertical black dashed lines correspond to the position of the maximum magnetic field.

The quasi-linear kinetic force model,  $R_{ei,quasi-linear}$ , has been extensively tested for different discharge parameters. This is shown in figure 10 where it is seen that the formula is in very good agreement with the measured friction force for each of the different simulation cases. This demonstrates that knowledge of the electron distribution function (or more specifically, of its derivative at the instability phase velocity) is crucial to properly quantifying the enhanced cross-field electron transport. One can also notice in figure 10 that the friction force exhibits a broad range of magnitudes (between 0.5 and 20 N.m<sup>-3</sup>) and diverse spatial profiles depending on the magnetic field and current density, and that the model given by equation 24 is able to capture all of this behaviour remarkably well given the complexity of the problem.

#### D. Ion-electron friction force

In some of the theoretical models discussed above, the anomalous force term is viewed as an instability-enhanced electron-ion friction force. This force term,  $F_{ei} = -R_{ei}$ , corresponds to a drag force between the electrons and ions that is formed due to the difference between the electron and ion drift velocities (and which is mediated by the instability electric field). If this term is truly a friction force however, then momentum conservation requires that the corresponding force term on the ions should be equal in magnitude, but opposite in direction. That is,  $R_{ie} = -R_{ei}$ . Figure 11 shows a comparison of the force terms  $R_{ei} = -q\langle\delta n_e\delta E_y\rangle$  and  $R_{ie} = q\langle\delta n_i\delta E_y\rangle$  computed directly in the PIC simulations. As seen, these force terms are in excellent agreement throughout the discharge, and for all of the simulation cases tested. Thus, the force term  $R_{ei}$  can indeed be viewed as an electron-ion friction force.

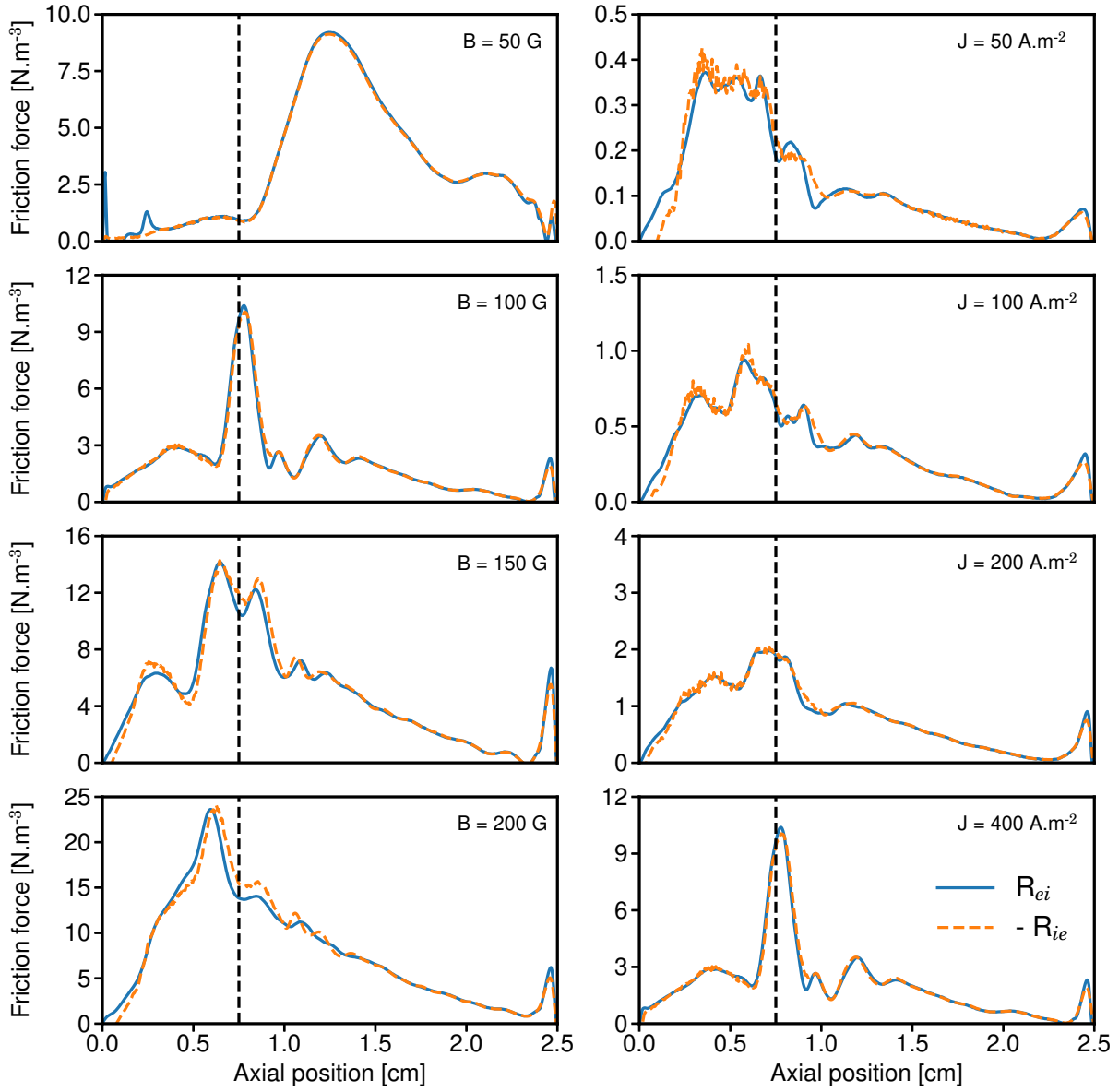


FIG. 11: Comparison between the azimuthal electron-ion and ion-electron force density terms for all of the simulation cases tested. The vertical black dashed lines correspond to the position of the maximum magnetic field.

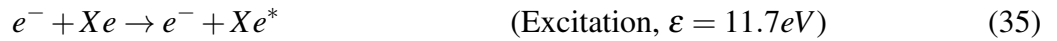
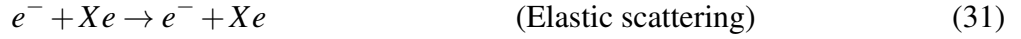
## V. ION-NEUTRAL COLLISIONS

For all the results shown in the previous sections, electron-neutral and ion-neutral collisions were not taken into account. In this section, we consider an imposed axial profile of the neutral density shown in figure 2(b). This profile has been obtained by solving the 1D Euler equations for

the neutral xenon gas, until a steady state is reached:

$$\begin{cases} \partial_t n_g + \partial_z(n_g v_g) = -S_{iz} \\ \partial_t(n_g v_g) + \partial_z(n_g v_g^2) = -\partial_z p_g - u_g S_{iz} \\ \partial_t(n_g E_g) + \partial_z(n_g E_g u_g) = -\partial_z(p_g u_g) \end{cases} \quad (30)$$

with  $n_g$ ,  $u_g$ ,  $p_g$  and  $E_g$  being respectively the neutral density, velocity, pressure and total energy, and  $S_{iz}$  the imposed ionization source term of figure 2(a). In this paper, a discharge current density of  $400 \text{ A.m}^{-2}$  is considered, which is lower than in "real" thrusters<sup>4</sup> with discharge current densities of around  $1000 \text{ A.m}^{-2}$ . Hence, to be consistent for the computation of the neutral density profile, the Xenon mass flow rate was set to  $1.5 \text{ mg.s}^{-1}$  with an inner and outer channel radius of 2 and 4 cm, respectively. In the PIC simulations, we also make use of a standard Monte Carlo Collision (MCC) module<sup>58</sup> to take into account the following collisions with neutral atoms:



The associated cross sections are taken from the LXCat database<sup>59</sup>. The ionization is still treated in a non-self-consistent way by using the imposed ionization source term shown in figure 2(a). No energy loss is taken into account and hence, the impact of the ionization process on the electrons is not analysed here. As described in Table I, three cases are simulated with inclusion of: only ion-neutral isotropic collisions (equation 36), only ion-neutral backscattering collisions (equation 37), or all of the ion-neutral and electron-neutral collisions detailed above.

The electron-ion friction force has been calculated for these 3 cases and its axial profile at steady-state is shown in figure 12, along with the nominal simulation case without any collisions. The friction force approximation of equation 24 is overlaid, where it can be seen that it still approximates very well the observed friction force. One can notice that this friction force (and

hence the axial electron transport) is greatly enhanced (by almost a factor 2) when all collisions (electron-neutral and ion-neutral) are taken into account. The ion-neutral isotropic scattering collisions do not have any significant effect on the friction force which stems from the fact that the corresponding collision frequency is low and no energy is exchanged. On the contrary, the ion-neutral backscattering collisions enhance the friction force, and hence play an important role for the axial transport. In figure 12(d), the electron-neutral momentum collisional drag force term has been displayed and we can notice that, as already observed in previous simulations<sup>35,60</sup>, the contribution of classical electron-neutral collisions to the axial electron transport is negligible compared to the electron-ion friction force.

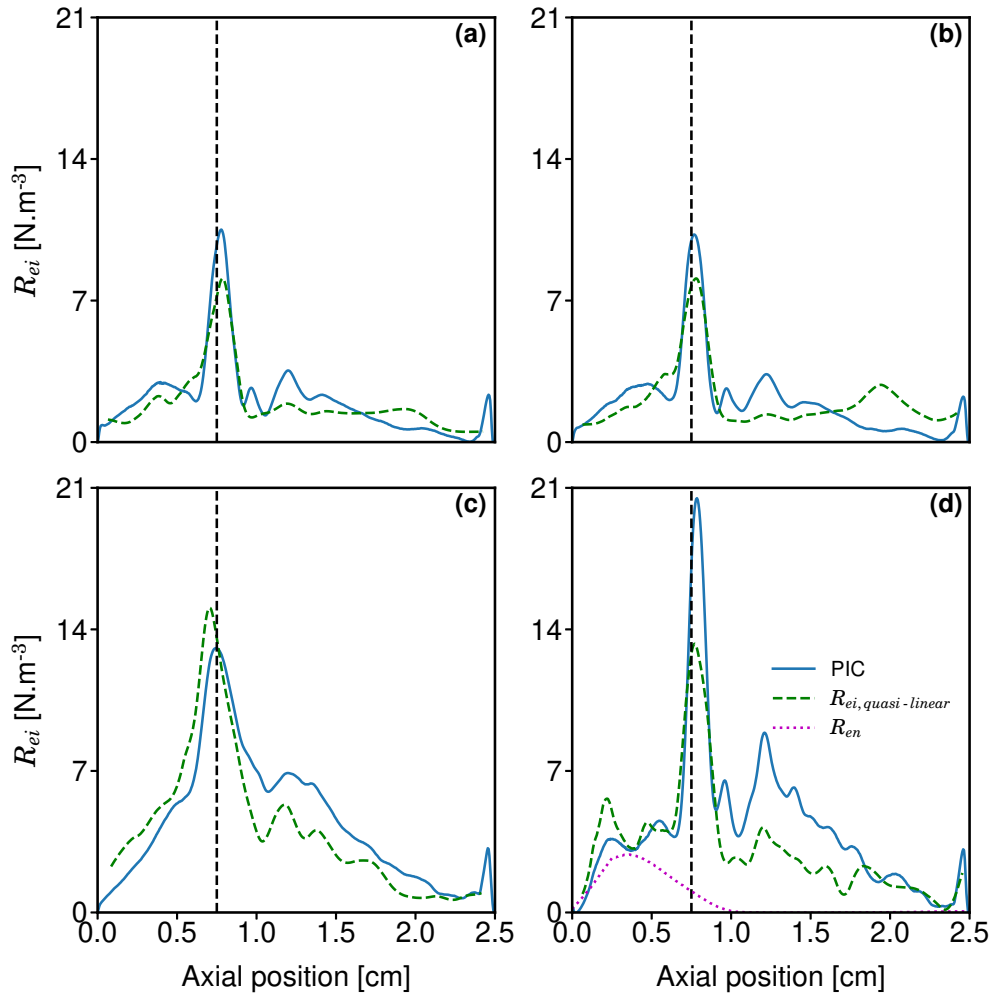


FIG. 12: Friction force approximation if: no collisions (i.e. nominal case) (a), only ion/neutral isotropic collisions (b) only ion/neutral backscattering collisions (c) all collisions electron/neutral and ion/neutral (d). Vertical black dashed lines correspond to the position of the maximum magnetic field.  $R_{en}$  correspond to the electron-neutral momentum collisional drag force term.

The electron-ion friction force enhancement by the ion-neutral backscattering collisions could be explained by considering the growth rate of the azimuthal instabilities,  $\gamma$ . A possible cause of damping for  $\gamma$  might be the linear Landau damping, as postulated in Ref. [7]. Charge-exchange collisions create low-energy ions from the main high-energy ion beam, and thus the ion velocity distribution is modified, which in turn is expected to change the instability growth rate. Indeed the wave energy density is found to increase when backscattering collisions are taken into account. The observation of low-energy ions contributing to the axial electron transport has already been observed by Katz *et al.*<sup>61</sup> in a simplified 2D axial-azimuthal PIC configuration.

The enhancement of the electron-ion friction force by electron-neutral collisions remains unclear, but may be related to a change in the electron distribution function (which then affects both the instability growth rate, and friction force). A deeper analysis is left for future work.

## VI. DISCUSSION AND CONCLUSION

A 2D axial-azimuthal Particle-In-Cell simulation model has been used as a baseline for extensive parametric studies. The radial magnetic field strength, discharge current density and neutral collisional processes have been varied, which gives a discharge that displays different instability behaviour and properties. These simulation results were used to challenge a recently developed theoretical model that quantifies the anomalous force leading to enhanced cross-field electron transport. Good agreement was obtained for all of the simulation cases tested. Hence, the kinetic theory appears to describe very well the anomalous transport, and the concept of this anomalous force as an electron-ion friction force was emphasized by showing that  $R_{ei} = -R_{ie}$ , i.e. this friction force does indeed correspond to a drag force between electrons and ions.

The theoretical model shows that the instability-enhanced friction force is very sensitive to the electron distribution function, which is in general strongly non-Maxwellian, and diverse in shape throughout the discharge. This explains the large challenge in modelling anomalous electron transport, and highlights the real difficulty in finding a first principles model that can be incorporated into a fluid simulation. Although the model was shown to be in good agreement with the simulation results and gives additional insight into the anomalous transport, it cannot yet be incorporated into a fluid simulation, as there is no self-consistent way to determine the electron velocity distribution function, or the instability wave energy density. While quasi-linear kinetic theory provides a relevant kinetic equation that can in principle be used to determine the distribution function,

this equation is very complicated and challenging to solve. Furthermore, if this equation could be solved, there would then be no need to actually use a fluid model since all relevant plasma properties could be obtained from moments of the distribution function itself. Aside from more detailed experimental measurements to confirm the importance of the instability-enhanced force, further theoretical work is needed to address these issues.

The validity of the quasi-linear approximation in the context of electron drift instabilities in HETs still requires further investigation. Even though in this work, the level of potential energy fluctuations does not exceed the ambient thermal energy of the plasma (which is often an approximate criterion for the validity of quasi-linear theory), nonlinear effects, such as ion-wave trapping, seem to be important. In the theoretical and numerical work by Lampe et al.<sup>47</sup>, the nonlinear regime considering electron magnetization was found to reduce to the linear regime with unmagnetized electrons. The large amplitude coherent waves cause electron scattering that smears out the electron cyclotron resonances, and leaves the plasma with an ion acoustic character. Since experimental measurements in HETs have observed linear dispersion relations consistent with such ion acoustic instabilities<sup>24,62</sup>, it appears that this result is valid. Although the quasi-linear model may not be complete, at present it appears to give very reasonable accuracy, and agrees with multiple, independent PIC simulations<sup>32,35,45</sup>.

The fact that the nominal simulation case has been simulated by 6 other research groups around the world, all obtaining similar results<sup>28</sup>, increases the confidence in the results obtained in the present work. They are also in agreement with previous axial-azimuthal PIC simulations using the same configuration and imposed ionization profile<sup>32</sup>, and similar to fully self-consistent simulations with no artificial ionization profile<sup>35</sup> (where good agreement with quasi-linear theory was also observed). Moreover, the instability fluctuation levels in the simulations now appear to be comparable with experimental measurements<sup>24,57</sup>. Further work is however needed to perform a more rigorous comparison, and to correctly account in the experiments for the observed spatial variation of these fluctuation levels in the simulations.

It has been observed that the nature of the predicted instabilities, and the resulting distribution of energy across different length scales, could be modified for longer azimuthal simulation lengths leading to an inverse energy cascade<sup>25,63,64</sup>. Although such a cascade has not been observed in recent axial-azimuthal simulations<sup>65</sup> similar to those used here, the role of the azimuthal length, and its impact, if any, on the electron drift instability needs to be clarified. The fact that the model is 2D and not 3D also precludes certain phenomena, such as electron loss on the radial

thruster walls, and intense secondary electron emission. However, aside from any possible issues associated with energy cascades, we think that the form of the quasi-linear model should still be valid in 3D since even though the electron distribution function may change, the model is anyway written in terms of the distribution function (which is to say that the enhanced electron transport will be naturally and automatically modified). Even though previous work with a self-consistent ionization source term<sup>29,60</sup> has shown that the quasi-linear theory remains valid, at least during the rising part of the discharge current during a breathing mode cycle, the imposed ionization source term used here nonetheless prevents the onset of these breathing mode oscillations; which could affect the growth of azimuthal instabilities during some moments of the discharge. This represents the next logical step in verifying the quasi-linear model, and is currently underway.

## Acknowledgements

T.C., A.T., P.C. and A.B. acknowledge support from the Agence Nationale de la Recherche under the reference ANR-16-CHIN-0003-01 and Safran Aircraft Engines within the project PO-SEIDON. They also acknowledge access to the HPC resources of CINES (under the allocation A0060510439 et A0040510092 made by GENCI) and of CERFACS at Toulouse.

## Data availability

The data that support the findings of this study are available from the corresponding author upon reasonable request.

## REFERENCES

- <sup>1</sup>P. Kelly and R. Arnell, *Vacuum* **56**, 159 (2000).
- <sup>2</sup>A. Revel, T. Minea, and C. Costin, *Plasma Sources Sci. Technol.* **27**, 105009 (2018).
- <sup>3</sup>A. I. Morozov, *Plasma Phys. Rep.* **29**, 235 (2003).
- <sup>4</sup>D. Goebel and I. Katz, *Fundamentals of Electric Propulsion: Ion and Hall Thrusters* (Wiley, Ney Jersey, 2008).
- <sup>5</sup>J. P. Boeuf and B. Chaudhury, *Phys. Rev. Lett.* **111**, 155005 (2013).

- <sup>6</sup>J. Cavalier, N. Lemoine, G. Bonhomme, S. Tsikata, C. Honore, and D. Gresillon, *Phys. Plasmas* **20**, 082107 (2013).
- <sup>7</sup>I. Katz, A. L. Ortega, B. Jorns, and I. G. Mikellides, in *52nd AIAA/SAE/ASEE Joint Propulsion Conference* (2016) pp. AIAA–4534.
- <sup>8</sup>A. Smolyakov, O. Chapurin, W. Frias Pombo, O. Koshkarov, I. Romadanov, T. Tang, M. Uman-sky, Y. Raitses, I. Kaganovich, and V. Lakhin, *Plasma Phys. Controlled Fusion* **59**, 014041 (2017).
- <sup>9</sup>J. Boeuf, *J. Appl. Phys.* **121**, 011101 (2017).
- <sup>10</sup>A. Powis, J. Carlsson, I. Kaganovich, Y. Raitses, and A. Smolyakov, *Phys. Plasmas* **25**, 072110 (2018).
- <sup>11</sup>K. Hara, *Plasma Sources Sci. Technol.* **28**, 044001 (2019).
- <sup>12</sup>F. Taccogna and L. Garrigues, *Reviews of Modern Plasma Physics* **3**, 12 (2019).
- <sup>13</sup>E. Choueiri, *Phys. Plasmas* **8**, 1411 (2001).
- <sup>14</sup>S. Mazouffre, *Plasma Sources Sci. Technol.* **22**, 013001 (2012).
- <sup>15</sup>J. Adam, J.-P. Boeuf, N. Dubuit, M. Dudeck, L. Garrigues, D. Gresillon, A. Heron, G. Hagelaar, V. Kulaev, N. Lemoine, S. Mazouffre, J. P. Luna, V. Pisarev, and S. Tsikata, *Plasma Phys. Control. Fusion* **50**, 124041 (2008).
- <sup>16</sup>S. Tsikata and T. Minea, *Phys. Rev. Lett.* **114**, 185001 (2015).
- <sup>17</sup>N. Meezan, W. H. Jr, and M. Cappelli, *Phys. Rev. E* **63**, 026410 (2001).
- <sup>18</sup>J. C. Adam, A. Heron, and G. Laval, *Phys. Plasmas* **11**, 295 (2004).
- <sup>19</sup>A. Ducrocq, J. C. Adam, A. Heron, and G. Laval, *Phys. Plasmas* **13**, 102111 (2006).
- <sup>20</sup>T. Lafleur, S. D. Baalrud, and P. Chabert, *Phys. Plasmas* **23**, 053503 (2016).
- <sup>21</sup>E. Chesta, C. M. Lam, N. B. Meezan, D. P. Schmidt, and M. A. Cappelli, *IEEE Transactions on Plasma Science* **29**, 582 (2001).
- <sup>22</sup>A. A. Litvak, Y. Raitses, and N. J. Fisch, *Phys. Plasmas* **11**, 1701 (2004).
- <sup>23</sup>A. Lazurenko, V. Vial, M. Prioul, and A. Bouchoule, *Phys. Plasmas* **12**, 013501 (2005).
- <sup>24</sup>S. Tsikata, N. Lemoine, V. Pisarev, and D. M. Grésillon, *Phys. Plasmas* **16**, 033506 (2009).
- <sup>25</sup>Z. A. Brown and B. A. Jorns, *Phys. Plasmas* **26**, 113504 (2019).
- <sup>26</sup>B. Vincent, S. Tsikata, S. Mazouffre, T. Minea, and J. Fils, *Plasma Sources Sci. Technol.* **27**, 055002 (2018).
- <sup>27</sup>I. G. Mikellides and A. L. Ortega, *Plasma Sources Sci. Technol.* **28**, 014003 (2019).

- <sup>28</sup>T. Charoy, J. P. Boeuf, A. Bourdon, J. A. Carlsson, P. Chabert, B. Cuenot, D. Eremin, L. Garrigues, K. Hara, I. D. Kaganovich, A. T. Powis, A. Smolyakov, D. Sydorenko, A. Tavant, O. Vermorel, and W. Villafana, *Plasma Sources Sci. Technol.* **28**, 105010 (2019).
- <sup>29</sup>T. Lafleur, R. Martorelli, P. Chabert, and A. Bourdon, *Phys. Plasmas* **25**, 061202 (2018).
- <sup>30</sup>J. J. Szabo, *Fully Kinetic Numerical Modeling of a Plasma Thruster*, Ph.D. thesis, Massachusetts Institute of Technology (2011).
- <sup>31</sup>P. Coche and L. Garrigues, *Phys. Plasmas* **21**, 023503 (2014).
- <sup>32</sup>J.-P. Boeuf and L. Garrigues, *Phys. Plasmas*. **25**, 061204 (2018).
- <sup>33</sup>W. M. Manheimer and J. P. Boris, *Phys. Rev. Lett.* **28**, 659 (1972).
- <sup>34</sup>S. Barral, K. Makowski, Z. Peradzyński, and M. Dudeck, *Phys. Plasmas* **12**, 073504 (2005).
- <sup>35</sup>T. Lafleur and P. Chabert, *Plasma Sources Sci. Technol.* **27**, 015003 (2018).
- <sup>36</sup>R. Davidson and N. Krall, *Nuclear Fusion* **17**, 1313 (1977).
- <sup>37</sup>T. Lafleur, S. D. Baalrud, and P. Chabert, *Plasma Sources Sci. Technol.* **26**, 024008 (2017).
- <sup>38</sup>A. Lenard, *Annals of Physics* **10**, 390 (1960).
- <sup>39</sup>R. Balescu, *The Physics of Fluids* **3**, 52 (1960).
- <sup>40</sup>G. Hagelaar, J. Bareilles, L. Garrigues, and J.-P. Boeuf, *Journal of Applied Physics* **93**, 67 (2003).
- <sup>41</sup>I. G. Mikellides, B. Jorns, I. Katz, and A. L. Ortega, in *52nd AIAA/SAE/ASEE Joint Propulsion Conference* (2016) pp. AIAA-4618.
- <sup>42</sup>B. Jorns, *Plasma Sources Sci. Technol.* **27**, 104007 (2018).
- <sup>43</sup>F. F. Chen, *Introduction to Plasma Physics and Controlled Fusion: Plasma Physics, 2nd ed.* (Plenum, New York, 1984).
- <sup>44</sup>J. Bareilles, G. J. M. Hagelaar, L. Garrigues, C. Boniface, J. P. Boeuf, and N. Gascon, *Phys. Plasmas* **11**, 3035 (2004).
- <sup>45</sup>V. Croes, T. Lafleur, Z. Bonaventura, A. Bourdon, and P. Chabert, *Plasma Sources Sci. Technol.* **26**, 034001 (2017).
- <sup>46</sup>A. Lazurenko, T. D. de Wit, C. Cavoit, V. Krasnoselskikh, A. Bouchoule, and M. Dudeck, *Phys. Plasmas* **14**, 033504 (2007).
- <sup>47</sup>M. Lampe, W. M. Manheimer, J. B. McBride, J. H. Orens, K. Papadopoulos, R. Shanny, and R. N. Sudan, *The Physics of Fluids* **15**, 662 (1972).
- <sup>48</sup>T. H. Stix., *Waves in plasmas* (AIP-Press, 1992).

- <sup>49</sup>E. V. A. A. Vedenov and R. Z. Sagdeev, in *International Conference on Plasma Physics and Controlled Thermonuclear Fusion* (Paper 199, 1961).
- <sup>50</sup>A. A. Vedenov, *Journal of Nuclear Energy. Part C, Plasma Physics, Accelerators, Thermonuclear Research* **5**, 169 (1963).
- <sup>51</sup>R. C. Davidson, *Methods in Nonlinear Plasma Theory* (Academic Press, New York and London).
- <sup>52</sup>S. D. Baalrud, C. C. Hegna, and J. D. Callen, *Phys. Rev. Lett.* **103**, 205002 (2009).
- <sup>53</sup>S. D. Baalrud, “Kinetic theory of instability-enhanced collective interactions in plasma,”.
- <sup>54</sup>A. Héron and J. C. Adam, *Phys. Plasmas* **20**, 082313 (2013).
- <sup>55</sup>J.-P. Boeuf, *Frontiers in Physics* **2**, 74 (2014).
- <sup>56</sup>T. Lafleur, S. D. Baalrud, and P. Chabert, *Phys. Plasmas* **23**, 053502 (2016).
- <sup>57</sup>S. Tsikata and K. Hara, in *29th International Electric Propulsion Conference, Vienna* (Paper A758, 2019).
- <sup>58</sup>V. Vahedi and M. Surendra, *Computer Physics Communications* **87**, 179 (1995).
- <sup>59</sup>A. V. Phelps, *Compilation of atomic and molecular data* (see [www.lxcat.net/Phelps](http://www.lxcat.net/Phelps), 2016).
- <sup>60</sup>T. Charoy, T. Lafleur, A. Tavant, A. Bourdon, and P. Chabert, in *29th International Electric Propulsion Conference, Vienna* (Paper A487, 2019).
- <sup>61</sup>I. Katz, V. H. Chaplin, and A. Lopez Ortega, *Phys. of Plasmas* **25**, 123504 (2018).
- <sup>62</sup>A. Lazurenko, G. Coduti, S. Mazouffre, and G. Bonhomme, *Phys. Plasmas* **15**, 034502 (2008).
- <sup>63</sup>S. Janhunen, A. Smolyakov, O. Chapurin, D. Sydorenko, I. Kaganovich, and Y. Raitses, *Phys. Plasmas* **25**, 011608 (2018).
- <sup>64</sup>Z. Asadi, F. Taccogna, and M. Sharifian, *Frontiers in Physics* **7**, 140 (2019).
- <sup>65</sup>J. A. Carlsson, I. D. Kaganovich, E. Rodriguez, Y. Raitses, and A. Smolyakov, in *29th International Electric Propulsion Conference, Vienna* (Paper A816, 2019).